

Solitary matter wave in spin-orbit-coupled Bose-Einstein condensates with helicoidal gauge potentialXiao-Xun Li, Rui-Jin Cheng, Ji-Li Ma, Ai-Xia Zhang, and Ju-Kui Xue^{*}*College of Physics and Electronics Engineering, Northwest Normal University, Lanzhou 730070, China*

(Received 17 January 2021; revised 3 September 2021; accepted 13 September 2021; published 21 September 2021)

We analytically and numerically study the different types of solitary wave in the two-component helicoidal spin-orbit coupled Bose-Einstein condensates (BECs). Adopting the multiscale perturbation method, we derive the analytical bright and dark solitary wave solutions of the system, and the stationary and moving bright (dark) solitary waves are obtained. The effects of spin-orbit coupling, the helicoidal gauge potential, the momentum, the Zeeman splitting, and the atomic interactions on the solitary wave types are discussed, and it is found that the coupling of these physical parameters can manipulate different types of solitary waves in the system. The results indicate that the helicoidal gauge potential breaks the symmetric properties of the energy band of the system and adjusts the energy band structure, thus further effecting the solitary wave properties, i.e., stationary or moving solitary wave, bright, or dark solitary wave. Correspondingly, the analytical predictions for exciting stationary or moving bright (dark) solitary wave in parameter space are obtained. In particular, the helicoidal gauge potential changes the solitary wave types drastically for the weak spin-orbit coupling, i.e., in the absence of the helicoidal gauge potential, only dark (bright) solitary wave solutions exist in the system with repulsive (attractive) atomic interaction; however, in the presence of the helicoidal gauge potential, both dark and bright solitary waves can exist in the system regardless of whether the atomic interaction is repulsive or attractive. In addition, we investigate the stability of solitary waves and obtain the stability regions of different types of solitary waves by applying the linear stability analysis. The dynamic evolution results of the solitary waves by the direct numerical simulation not only validate the linear stability analysis but also confirm the analytical prediction of the solitary waves. Finally, the collision effects between solitary waves are also presented by the numerical simulation. It is shown that the interactions between solitary waves in the system have both elastic and inelastic collisions, which are closely related to the position of solitary wave states in the linear energy band. Our results provide a potential way to adjust the types of solitary waves in BECs with helicoidal gauge potential.

DOI: [10.1103/PhysRevE.104.034214](https://doi.org/10.1103/PhysRevE.104.034214)**I. INTRODUCTION**

Solitary waves are one of the most important topics in nonlinear systems. The solitary waves are localized wave packets that can propagate at a constant velocity without changing their shape due to the balancing between the dispersion and nonlinear effects [1]. Solitons are solitary waves that emerge unscathed from collisions with each other, up to shifts in position and phase; this is reminiscent of particle behavior, motivating the particle-like name soliton [2]. Solitary waves and solitons play a significant role in many branches of physics and have been observed and investigated in various fields, such as water waves [3], plasma physics [4], nonlinear optics [5], and Bose-Einstein condensates (BECs) [6,7]. Among the various systems that support solitary waves, BECs provide an ideal platform for exploring the properties of solitary waves because of its clean and parameter-controllable characteristics [8]. Therefore, experimental and theoretical research concerning the nonlinear evolution of solitary waves in BECs have been attracted more and more attention. In the case of single-component BEC, solitary waves have been investigated in many works, the system can have bright (dark)

solitary wave solutions for attractive (repulsive) interatomic interactions, respectively [9,10]. In the two-component BECs, many combined vector solitons have been obtained, such as dark-dark solitons [11], bright-bright solitons [12], dark-bright solitons [13], and dark-antidark solitons [14].

Since the experimental implementation of spin-orbit (SO) coupling in BECs, it has stimulated the extensive investigation of the properties of SO coupled BECs. The SO coupling not only introduces more tunable parameters, but also brings richer soliton structures, including striped solitons [15–17], gap solitons [18–21], gray solitons [22], and semivortex and mixed-mode solitons [23–25]. By using a multiscale perturbation method, the effects of SO coupling on solitary wave properties in the two-component BECs have been studied. For instance, three distinct states of bright soliton having zero momentum, finite momentum, and stripe densities are found in SO coupled BECs with attractive interactions [15]. Beyond this, the different types of solitary wave in such SO coupled BECs are also presented in a unified description, and the approximate bright and dark solitary wave solutions are obtained for attractive and repulsive interatomic interactions, respectively [26]. In addition, the solitary waves in SO coupled spinor BECs have been studied by the same method [27,28].

^{*}Corresponding author: xuejk@nwnu.edu.cn

Gauge potential is ubiquitous in various fields and can be generated artificially in atomic systems. The potential of practically arbitrary form can be designed by a proper combination of laser beams in atomic systems, which is possible to engineer SO coupling in BECs [29–31]. Recently, the inhomogeneous gauge field in BECs is a growing topic of interest [32–37], based on the tunable SO coupling in atomic systems and the intrinsic nonlinearity of SO coupled BECs [38–42], the soliton dynamics in SO coupled BECs with inhomogeneous gauge potential have been extensively studied [34–37]. The soliton complexes and spinor dynamics in localized SO coupled BECs with a particular inhomogeneous gauge potential has been studied [34]. The dynamics of spinor solitons were proposed in the self-attractive SO coupled BECs with arbitrary potentials [35]. In particular, a helicoidal gauge potential can be implemented in the experiment through the light propagation in the helical waveguide array [43], and the studies [36,37] have shown that it has an important influence on the solitary wave excitation in SO coupled BECs. In the spatially inhomogeneous BECs with helicoidal SO coupling, the existence and stability of families of steadily moving solitary waves are investigated [36]. For the attractive two-dimensional spinor BECs with helicoidal spatially periodic SO coupling, the system supports a rich variety of stable fundamental solitons and bound soliton complexes, and the helicoidal SO coupling can make their bound states stable [37].

Although the solitary waves in helicoidal SO coupled BECs have been discussed in the previous studies, there is still lacking with the detailed exploration of the mechanism of different types of solitary waves caused by the helicoidal gauge potential. In particular, the theoretical evidence for manipulating solitary wave types in parameter space by utilizing the helicoidal gauge potential is unclear. Considering this is also an important and worthwhile topic, so in this paper, we investigate the excitation of different types of solitary wave in the two-component helicoidal SO coupled BECs by using the multiscale perturbation method. This method allows derivation of a single nonlinear Schrödinger (NLS) equation which can obtain the analytical solitary wave solutions in the system by starting from the one-dimensional helicoidal SO coupled two-component Gross-Pitaevskii (GP) equations. The influence of different physical parameters on the solitary wave types is analyzed in detail, and the stationary or moving bright (dark) solitary wave in parameters space is predicted analytically. In addition, we find that the helicoidal gauge potential plays an important role on the solitary wave types in the system. The helicoidal gauge potential breaks the symmetric properties of the energy band of the system. And it can drastically change the solitary wave types in the system for the weak spin-orbit coupling. Finally, the stabilities and collision effects of solitary waves are also investigated by the linear stability analysis and numerical simulation.

The paper is structured as follows. In Sec. II, we describe the theoretical model of the two-component BECs with helicoidal SO coupling and deduce the single NLS equation. In Sec. III, the types of solitary wave are analysed in detail. In Sec. IV, the stabilities and collision effects of the solitary waves are studied by the linear stability analysis and the numerical simulation. The paper is concluded in Sec. V.

II. THE MODEL AND DERIVATION OF NLS EQUATION

We consider a one-dimensional spatially inhomogeneous two-component BECs with helicoidal SO coupling in the presence of atomic interactions, the dimensionless GP equations describing the spinor wave function $\Psi = (\Psi_1, \Psi_2)^T$ can be expressed as follows [36,44]:

$$i \frac{\partial \Psi}{\partial t} = \frac{1}{2} \left[\frac{1}{i} \frac{\partial}{\partial x} + \alpha A(x) \right]^2 \Psi + \frac{\Delta}{2} \sigma_z \Psi + G \Psi, \quad (1)$$

where $A(x)$ is the spatially varying gauge potential; α is the potential amplitude; Δ is the Zeeman splitting; $\sigma_{x,y,z}$ are Pauli matrices; and the spatial variable x , time t , density $|\Psi|^2$, and energy are expressed in normalized units $a_{\perp} = \sqrt{\hbar/(m\omega_{\perp})}$, ω_{\perp}^{-1} (ω_{\perp} is the transverse trap frequency), a_{\perp}^{-1} , and $\hbar\omega_{\perp}$, respectively; and m is the atomic mass. Here $G = \text{diag}(g_1|\Psi_1|^2 + g_{12}|\Psi_2|^2, g_2|\Psi_2|^2 + g_{12}|\Psi_1|^2)$ characterizes the interatomic interaction with the interaction constants $g_{1,2} \equiv 2a_{1,2}/a_{\perp}$ and $g_{12} \equiv 2a_{12}/a_{\perp}$. The $a_{1,2}$ and a_{12} are s -wave scattering length, they can be controlled by optical and magnetic Feshbach resonance techniques in actual experiments [45,46].

The helicoidal SO coupling $A(x) = \boldsymbol{\sigma} \cdot \mathbf{n}(x)$, where $\mathbf{n}(x) = [\cos(2\beta x), \sin(2\beta x), 0]$ and $\boldsymbol{\sigma} = (\sigma_x, \sigma_y, \sigma_z)$. β is the frequency of rotation, the positive and negative values of β are defined for right-handed mode and left-handed mode, respectively [43,47,48]. The helicoidal structure of the vector potential is point translational symmetry (the shift by the period π/β). For convenience, we use gauge transformation $\Psi = e^{-i(\alpha^2 + \beta^2)t/2} e^{-i\sigma_z \beta x} \psi$ to switch to the rotating frame for the chosen gauge field $A(x)$ [36,44], then the point translation symmetry of Eq. (1) becomes continuous translational symmetry of the transformed equations, and the continuous GP equations for ψ are

$$i \frac{\partial \psi_1}{\partial t} = -\frac{1}{2} \frac{\partial^2 \psi_1}{\partial x^2} + i\beta \frac{\partial \psi_1}{\partial x} - i\alpha \frac{\partial \psi_2}{\partial x} + \frac{\Delta}{2} \psi_1 + (g_1|\psi_1|^2 + g_{12}|\psi_2|^2)\psi_1, \quad (2)$$

$$i \frac{\partial \psi_2}{\partial t} = -\frac{1}{2} \frac{\partial^2 \psi_2}{\partial x^2} - i\beta \frac{\partial \psi_2}{\partial x} - i\alpha \frac{\partial \psi_1}{\partial x} - \frac{\Delta}{2} \psi_2 + (g_2|\psi_2|^2 + g_{12}|\psi_1|^2)\psi_2, \quad (3)$$

where α represents the SO coupling and β represents the helicoidal gauge potential. The number of atoms in each component is given by $N_j = \int_{-\infty}^{+\infty} |\psi_j|^2 dx$, $j = 1, 2$. The stationary counterpart of Eqs. (2) and (3) is obtained by factorizing $\psi(x, t) = \varphi(x) e^{-i\mu t}$, where μ denotes the chemical potential.

Many methods in experiment could generate solitary wave, such as phase imprinting method [49,50] and modulational instability [9]. In these experiments, the observed solitary waves belong to weakly nonlinear excitations on the condensate background. The multiscale perturbation method [15,17,26,51] is reasonable and very effective on the study of weakly nonlinear excitation on the background. Furthermore, this method utilizes proper scales and asymptotic expansions to reduce the original model into a single NLS equation. Such a reduction allows us to derive approximate analytical bright and dark solitary wave solutions with positive or negative

mass, depending on the type of the effective dispersion and nonlinear interaction. We derive approximate solitary wave solutions of Eqs. (2) and (3) via a multiscale perturbation method. To proceed, we seek solutions to Eqs. (2) and (3) of the form

$$\psi = \sum_{n=1}^{\infty} \epsilon^n \mathbf{u}_n e^{i(kx - \mu t)} = \sum_{n=1}^{\infty} \epsilon^n \begin{pmatrix} U_n \\ V_n \end{pmatrix} \phi_n e^{i(kx - \mu t)}, \quad (4)$$

where the vectors $\mathbf{u}_n = [U_n, V_n]^T \phi_n$ are composed by the coefficients U_n, V_n and the unknown field envelopes $\phi_n \equiv \phi_n(T, X)$. $\phi_n(T, X)$ are assumed to be functions of the slow variables $T = \epsilon^2 t$ and $X = \epsilon(x - vt)$, where v is the group velocity. ϵ (ϵ is a dimensionless small parameter, $0 < \epsilon \ll 1$) reflects the intensity of weak excitation and represents the perturbation amplitude. Additionally, k is the momentum, $\mu = \omega + \epsilon^2 \omega_0$ is the chemical potential, here ω is the energy in the linear limit, and $\epsilon^2 \omega_0$ is a small deviation about this energy [$\omega_0/\omega = O(1)$].

Substituting Eq. (4) into Eqs. (2) and (3), we obtain these equations at $O(\epsilon)$, $O(\epsilon^2)$, and $O(\epsilon^3)$, respectively:

$$\mathbf{A} \mathbf{u}_1 = 0, \quad (5)$$

$$\mathbf{A} \mathbf{u}_2 = i \mathbf{A}_0 \partial_x \mathbf{u}_1, \quad (6)$$

$$\mathbf{A} \mathbf{u}_3 = i \mathbf{A}_0 \partial_x \mathbf{u}_2 - i(\partial_T + \frac{1}{2} \partial_x^2 - \mathbf{B} + \omega_0) \mathbf{u}_1, \quad (7)$$

where matrices \mathbf{A} , \mathbf{A}_0 , and \mathbf{B} are defined as follows:

$$\mathbf{A} = \begin{pmatrix} \omega - \frac{k^2}{2} + k\beta - \frac{\Delta}{2} & -k\alpha \\ -k\alpha & \omega - \frac{k^2}{2} - k\beta + \frac{\Delta}{2} \end{pmatrix}, \quad (8)$$

$$\mathbf{A}_0 = \begin{pmatrix} v - k + \beta & -\alpha \\ -\alpha & v - k - \beta \end{pmatrix}, \quad (9)$$

$$\mathbf{B} = \begin{pmatrix} g_1 U_1^2 |\phi_1^2| + g_{12} V_1^2 |\phi_1^2| & 0 \\ 0 & g_2 V_1^2 |\phi_1^2| + g_{12} U_1^2 |\phi_1^2| \end{pmatrix}. \quad (10)$$

At $O(\epsilon)$, Eq. (5) indicates that the solvability condition $\det(\mathbf{A}) = 0$ yields the linear excitation energy spectrum

$$\omega = \omega_{\pm}(k) = \frac{k^2}{2} \pm \sqrt{k^2 \alpha^2 + \left(\beta k - \frac{\Delta}{2}\right)^2}. \quad (11)$$

Although solitary waves may also exist in an excited state occupying simultaneously each energy band, we will only investigate nonlinear states in the form of solitary wave, which correspond to the lower-energy band ω_- . Note that the lower-energy band ω_- has different behaviors depending on the external physical parameters. We can obtain the distribution of the energy branch ω_- in momentum space k , and the results for changing the Zeeman splitting Δ and the helicoidal gauge potential β under given SO coupling α are shown in Fig. 1.

As shown in Fig. 1(a), in the absence of the helicoidal gauge potential ($\beta = 0$), the lower-energy band $\omega_-(k)$ has a double-well structure in the case of $\Delta < 2\alpha^2$ and there are two minima at $k = \pm k_0 = \pm \sqrt{4\alpha^4 - \Delta^2}/2\alpha$. However, $\omega_-(k)$ has a single-well structure in the case of $\Delta > 2\alpha^2$ and there is one minimum at $k = 0$. In this case, the energy band

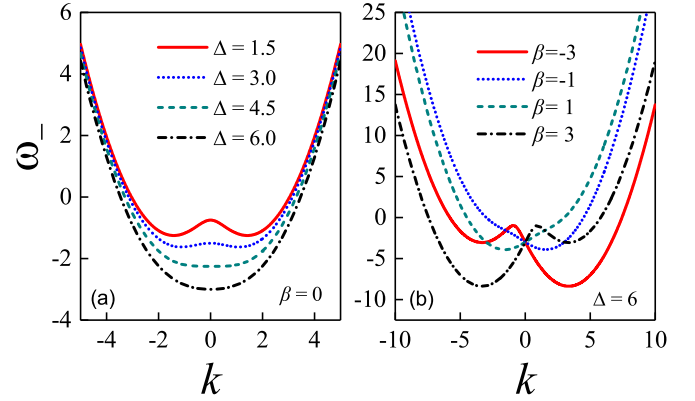


FIG. 1. The lower branch of the linear energy spectrum: (a) for different Zeeman splitting Δ with $\beta = 0$ and (b) for different helicoidal gauge potential β with $\Delta = 6$. Here $\alpha = 1.5$.

structure of the system is symmetric about the momentum $k = 0$. Moreover, the lower-energy band $\omega_-(k)$ of the system changes from a double-well structure to a single-well structure with the increase of the Zeeman splitting Δ . Interestingly, the symmetry structure of the lower-energy band $\omega_-(k)$ will be broken in the presence of the helicoidal gauge potential ($\beta \neq 0$), this is clearly shown in Fig. 1(b). It can also be seen that the lower-energy band $\omega_-(k)$ of the system changes from a single-well structure to a double-well structure with the increase of the helicoidal gauge potential $|\beta|$, and it is symmetric about the momentum $k = 0$ for the right-handed and left-handed helicoidal gauge potential.

Then, the solution of the first-order equation $O(\epsilon)$ is written as

$$\mathbf{u}_1 = \begin{pmatrix} U_1 \\ V_1 \end{pmatrix} \phi_1(X, T) = \begin{pmatrix} 1 \\ Q \end{pmatrix} \phi_1(X, T), \quad (12)$$

where the parameter Q is given by

$$Q = \left(\omega - \frac{k^2}{2} + k\beta - \frac{\Delta}{2} \right) / k\alpha. \quad (13)$$

Note that the above parameter sets the left and right eigenvectors of \mathbf{A} at 0 eigenvalue, being given by $\mathbf{L} = [1, Q]$ and $\mathbf{R} = [1, Q]^T$, respectively.

At the order $O(\epsilon^2)$, using the compatibility condition of Eq. (6), $\mathbf{L} \mathbf{A}_0 \mathbf{R} = 0$, the group velocity is obtained

$$v = \frac{\partial \omega}{\partial k} = k - \frac{2k\alpha^2 + 2\beta(k\beta - \frac{\Delta}{2})}{2\sqrt{k^2\alpha^2 + (k\beta - \frac{\Delta}{2})^2}}. \quad (14)$$

It is clear that v is substantially influenced by the Zeeman splitting Δ , the SO coupling α , the helicoidal gauge potential β , and the momentum k .

Using Eq. (12), we can also obtain the form of the solution for \mathbf{u}_2 :

$$\mathbf{u}_2 = -i \left[Q + (2kv - k^2 - 2\omega + \Delta)/2k^2\alpha \right] \frac{\partial \phi_1}{\partial X}. \quad (15)$$

Finally, we consider $O(\epsilon^3)$. Taking advantage of the compatibility condition for Eq. (5), i.e., $\det(\mathbf{A}) = 0$, together with Eqs. (12) and (15), we eliminate the third-order terms \mathbf{u}_3 from

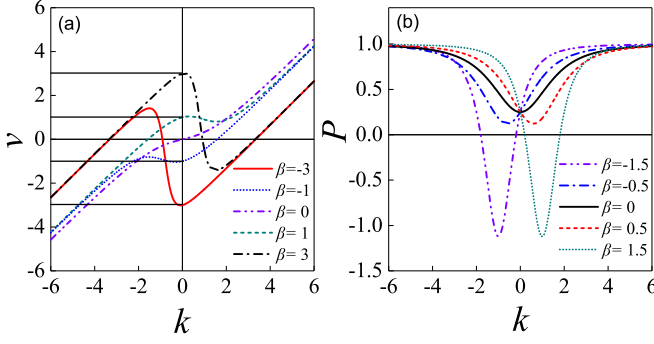


FIG. 2. Distribution of (a) group velocity v and (b) dispersion coefficient P of different helical gauge potential β in momentum k space. The other parameters $\alpha = 1.5$, $\Delta = 6$.

Eq. (7) and obtain a single NLS equation for the unknown field envelope $\phi_1 = \phi$:

$$i \frac{\partial \phi}{\partial T} = -\frac{1}{2} P \frac{\partial^2 \phi}{\partial X^2} + S |\phi|^2 \phi - \omega_0 \phi, \quad (16)$$

where the coefficients are given by

$$P = \frac{\partial^2 \omega}{\partial k^2} = 1 + \{4Q\alpha + (2kv - k^2 - 2\omega + \Delta)/k^2 - 2(v - k + \beta) - (v - k - \beta)(2kv - k^2 - 2\omega + \Delta)Q/k^2\alpha + 2Q^2\}/(1 + Q^2), \quad (17)$$

$$S = \frac{g_1 + 2g_{12}Q^2 + g_2Q^4}{1 + Q^2}. \quad (18)$$

III. ANALYSIS OF THE SOLITARY WAVES

In this section, we will focus on the solitary waves corresponding to the lower-energy band. Based on the analysis of the systematic energy band structure in the previous section, we also plot the group velocity v as a function of the momentum k in Fig. 2(a) corresponding to Fig. 1. When v is zero, we can obtain stationary solitary waves; however, when v is nonzero, moving solitary waves can be obtained. It can be seen from Fig. 2(a) that the variation of group velocity v with the momentum k is linear in the absence of the helicoidal gauge potential ($\beta = 0$), and has a nonlinear oscillation character near the momentum $k = 0$ in the presence of β . Furthermore, the group velocity $v = \beta$ [see Eq. (14)] is no longer zero at $k = 0$ when $\beta \neq 0$. We can also see that v for the right-handed and left-handed helicoidal gauge potential β shows a large difference when the value of $|k|$ is small; however, it will become consistent with larger $|k|$. It can also be observed from Fig. 2(a) that the number of the points at which $v(k) = 0$ [i.e., the number of points at which the curve $v = v(k)$ intersects the $v = 0$ axis] can be changed from 1 to 3 as the strength of $|\beta|$ increases, which means that the value of β can significantly affect the number of stationary solitary waves in the system.

In order to further analyze the influence of β on the number of stationary solitary waves in the system, we also plot the dispersion coefficient P with the momentum k in Fig. 2(b) because of $P = \partial v / \partial k$, where the values of α and Δ are the

same as those in Fig. 2(a). From $\partial P / \partial k = 0$, the minimum value of P is obtained when $k = \beta \Delta / [2(\alpha^2 + \beta^2)]$ as $P_{\min} = 1 - 2\sqrt{(\alpha^2 + \beta^2)^3} / \sqrt{\alpha^2 \Delta^2}$. Setting $P_{\min} = 0$, we can obtain

$$\beta^2 = C_0 = \sqrt[3]{\frac{\alpha^2 \Delta^2}{4}} - \alpha^2. \quad (19)$$

Next, we will discuss that according to the positive and negative value of P_{\min} in the following two cases.

(a) When $\beta^2 \leq C_0$, $P_{\min} \geq 0$ is constant [e.g., the black, red and blue lines in Fig. 2(b)]. In this case, the relationship between v and k is always linear and the curve $v = v(k)$ intersects the $v = 0$ axis at one point, which means that there is only one stationary solitary wave in the system [e.g., the purple line in Fig. 2(a)].

(b) When $\beta^2 > C_0$, $P_{\min} < 0$, there exists intervals of momenta for $P > 0$ and $P < 0$ simultaneously [e.g., the purple and green lines in Fig. 2(b)], where we set the momentum value k for $P = 0$ as k_A, k_B . Correspondingly, there are two extrema of v , which are set as $v(k_A)$ and $v(k_B)$, respectively. Note that the number of the points at which $v(k) = 0$ in the v - k plane, i.e., the number of stationary solitary waves in the system, is closely related to the value of $v(k_A)v(k_B)$, which can be discussed into the following three cases:

(i) When $v(k_A)v(k_B) > 0$, there exists only one point at which $v(k) = 0$ in the v - k plane and the system has one stationary solitary wave.

(ii) When $v(k_A)v(k_B) = 0$, there are two points at which $v(k) = 0$ in the v - k plane. However, one of the points corresponds to an extreme point of $v(k)$, then the dispersion coefficient $P = \partial v / \partial k = 0$ in the NLS equation, so naturally there is no solitary wave solution. Therefore, in this case, the system still has only one stationary solitary wave.

(iii) When $v(k_A)v(k_B) < 0$, there are three points at which $v(k) = 0$ in v - k plane and the system has three stationary solitary waves.

In the following, we will concretely obtain the parameter space of the number of stationary solitary wave in the system according to the above three cases. From $P = 0$, we can obtain

$$k_{A,B} = \frac{\beta \Delta \mp \sqrt{3\sqrt{4\alpha^4 \Delta^4 (\alpha^2 + \beta^2)} - \alpha^2 \Delta^2}}{2(\alpha^2 + \beta^2)}. \quad (20)$$

Substituting Eq. (20) into Eq. (14), and then $v(k_A)v(k_B) = 0$ can be expressed as

$$-4(\alpha^2 + \beta^2)^2 + 6\sqrt{2\alpha^2 \Delta^2}(\alpha^2 + \beta^2) + \Delta^2 - 3\sqrt[3]{4\alpha^4 \Delta^4} = 0. \quad (21)$$

It can be seen that Eq. (21) is a quadratic equation with one variable about β^2 , and its corresponding function image is downward. Solving Eq. (21), we can obtain the analytical results

$$\beta^2 = C_{1,2} = -\alpha^2 + \frac{3\sqrt[3]{2\alpha^2 \Delta^2}}{4} \mp \frac{\sqrt{4\Delta^2 - 3\sqrt[3]{4\alpha^4 \Delta^4}}}{4}. \quad (22)$$

According to Eq. (22), when $\Delta < 3\sqrt{3}/4\alpha^2$, $C_{1,2}$ have no real solutions and $v(k_A)v(k_B) < 0$, corresponding to the case (iii), the system has three stationary solitary waves. When $\Delta \geq$

TABLE I. Summary of the Stationary Solitary Wave Numbers in Helicoidal SO Coupled BECs.

$\Delta \neq 0$					$\Delta = 0$
$\beta^2 > C_0$			$\beta^2 \leq C_0$		2
$\Delta < 3\sqrt{3}\alpha^2/4$	$3\sqrt{3}\alpha^2/4 \leq \Delta < 2\alpha^2$	$\Delta \geq 2\alpha^2$			
	$\beta^2 < C_1$ or $\beta^2 > C_2$	3	$\beta^2 > C_2$	3	
3	$C_1 \leq \beta^2 \leq C_2$	1	$\beta^2 \leq C_2$	1	

$3\sqrt{3}/4\alpha^2$, $C_{1,2}$ have real solutions. Here it can be obtained from the calculation that $C_2 > C_0$ is inevitable. However, the relationship between C_0 and C_1 can be divided into the following two cases. When $C_1 > C_0$ (i.e., $3\sqrt{3}/4\alpha^2 \leq \Delta < 2\alpha^2$), then $v(k_A)v(k_B) \geq 0$ when $C_1 \leq \beta^2 \leq C_2$ corresponding to the case (i) and (ii), and $v(k_A)v(k_B) < 0$ when $\beta^2 < C_1$ or $\beta^2 > C_2$ corresponding to the case (iii). When $C_1 \leq C_0$ (i.e., $\Delta \geq 2\alpha^2$), then $v(k_A)v(k_B) < 0$ when $\beta^2 > C_2$ corresponding to the case (iii), and $v(k_A)v(k_B) \geq 0$ when $\beta^2 \leq C_2$ corresponding to the case (i) and (ii). Through the above calculation, we can obtain the number of stationary solitary waves in momentum space k and the summary are shown in Table I. The results given in Table I are further confirmed in Fig. 2. As Fig. 2(a) shows, when $\Delta = 6$, $\alpha = 1.5$, $\Delta \geq 2\alpha^2$, and $C_2 \simeq 3.69$, it can be seen from Table I that when $\beta = \pm 1$, $\beta^2 < C_2$, the system has one stationary solitary wave; when $\beta = \pm 3$, $\beta^2 > C_2$, the system has three stationary solitary waves. In particular, when $\Delta = 2\alpha^2$, it can be obtained from Eq. (22) that $C_1 = 0$, $C_2 = \alpha^2$. In this case, there has one stationary solitary wave when $|\beta| \leq \alpha$ and three stationary solitary waves when $|\beta| > \alpha$. In addition, when $\Delta = 0$, it can be obtained from Eq. (14) that there are always two stationary solitary waves in the system at $k = \pm\sqrt{\alpha^2 + \beta^2}$, and this result is consistent with that in Ref. [36].

To further explore the coupled effects of the SO coupling and the helicoidal gauge potential on the group velocity v , Fig. 3 illustrates $v = 0$ in the α - β plane for different momenta k . It is clear that when $\beta = 0$, the system has always two stationary solitary waves at $\alpha = \pm\sqrt{(k^2 + \sqrt{k^4 + \Delta^2})/2}$ [see Eq. (14)]. Note that the change of β can significantly affect the number of stationary solitary waves in the α space, which may be 0, 1, 2, 3, or 4. It can also see from Fig. 3 that the plot of $v = 0$ in the α - β plane is asymmetric about $\beta = 0$ when $|k|$ is small, and it is different for the positive and negative k . However, with the increase of k , the plot will become symmetric gradually about $\beta = 0$ and will become consistent for the positive and negative k . Furthermore, it is noted that the plot of $v = 0$ is always symmetric about $\alpha = 0$ in the α - β plane, and the regions of $v > 0$ ($k > 0$) and $v < 0$ ($k < 0$) gradually diffuses outward with the increase of momentum $|k|$.

Now we analyze different types of solitary waves in the system. It is known that the effective NLS equation (16) has solitary wave solutions, and the sign of the dispersion P and nonlinearity S of Eq. (16) is crucial in determining the types of solitary waves. When the signs of P and S are same, i.e., $PS > 0$, the system exists dark solitary waves. When the signs

are opposite, i.e., $PS < 0$, the system exists the bright solitary waves. Note that dark solitary waves exist inside the linear band ($\omega_0 > 0$), while the bright solitary waves are found in the infinite gap below the lower-energy band ($\omega_0 < 0$) [15,17,26]. Generally, when the dispersion coefficient $P > 0$ ($P < 0$), the solitary wave is called positive (negative) mass solitary waves. As can be seen from the Eq. (18), the sign of S mainly depends on the atomic interactions, and the repulsive (attractive) atomic interactions correspond to $S > 0$ ($S < 0$) respectively. Unlike S , the sign of P is determined by the coupled effects of α , β , Δ , and k . In the presence of the Zeeman splitting Δ , $P > 0$ when $\beta^2 < C_0$, which means that the system exists the positive mass dark ($S > 0$) or bright ($S < 0$) solitary waves in this case; when $\beta^2 > C_0$, $P > 0$ and $P < 0$ coexist in the momentum space k , thus there exist the positive mass dark solitary waves ($P > 0$, $S > 0$), the positive mass bright solitary waves ($P > 0$, $S < 0$), the negative mass dark solitary waves ($P < 0$, $S < 0$), and the negative mass bright solitary waves ($P < 0$, $S > 0$). Specifically, in the absence of the Zeeman splitting ($\Delta = 0$), the dispersion coefficient $P = 1 > 0$ is a constant, and there exist the positive mass dark ($S > 0$) or bright ($S < 0$) solitary waves.

In Fig. 4, the dark and bright solitary wave regions in the α - β plane are shown for different k , which are obtained by plotting $PS = 0$. Interestingly, the helicoidal gauge potential β changes the solitary wave types drastically for the weak SO

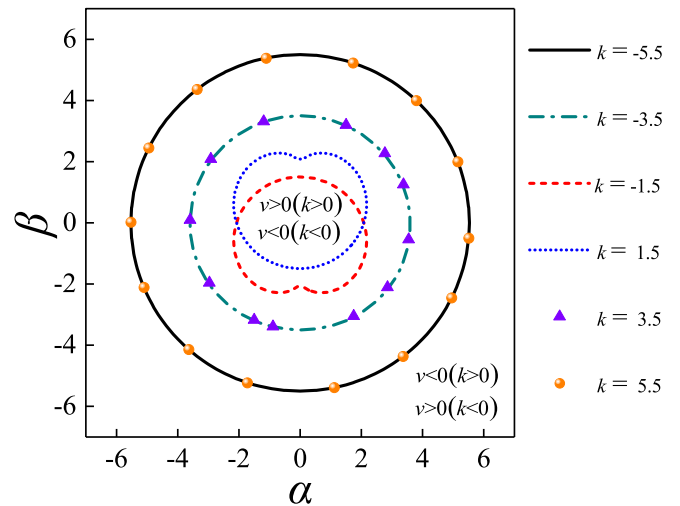


FIG. 3. The group velocity region (i.e., $v < 0$, $v = 0$, $v > 0$) for different k in α - β plane. Here $\Delta = 6$.

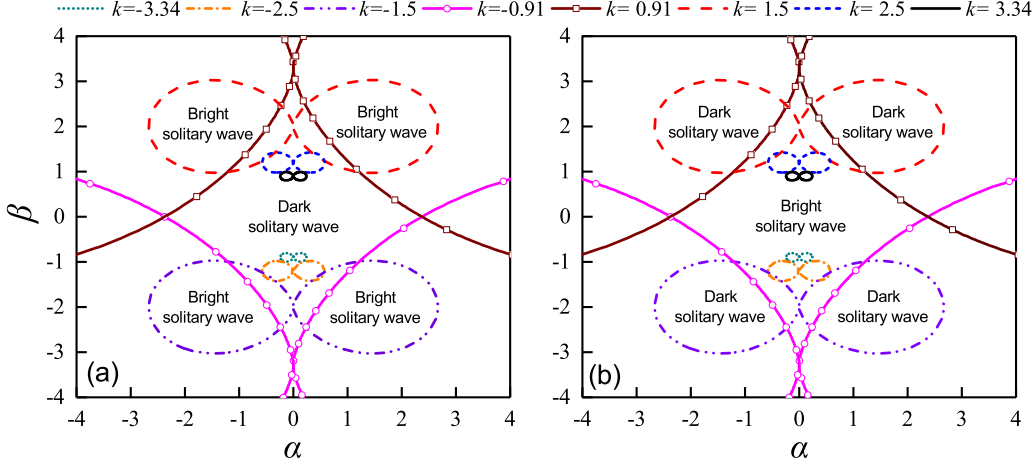


FIG. 4. Bright and dark solitary wave regions for different k in α - β plane. (a) $S > 0$ with $g_1 = g_2 = g_{12} = 1$. (b) $S < 0$ with $g_1 = g_2 = g_{12} = -1$. Here $\Delta = 6$.

coupling, i.e., when $\beta = 0$, only dark (bright) solitary wave solutions exist in the system with repulsive (attractive) atomic interaction; however, when $\beta \neq 0$, both dark and bright solitary waves can exist in the system regardless of whether the atomic interaction is repulsive or attractive. As can be seen from Fig. 4(a), with the repulsive atomic interactions (i.e., $S > 0$), the bright solitary wave region in the α - β plane presents lemniscates and is always symmetrical about $\alpha = 0$ and decreases with the increase of momentum $|k|$. Clearly, when $|k|$ is sufficiently large, only dark solitary wave solutions exist. It can also be found that the bright and dark solitary wave regions of the system are also symmetrical about $\beta = 0$ for $\pm k$. Meanwhile, the bright solitary waves mainly appear in the region of $\beta > 0$ ($\beta < 0$) for the positive (negative) momentum k . Figure 4(b) illustrates that the region of dark and bright solitary waves with the attractive interactions (i.e., $S < 0$) is just opposite to that when the interaction is repulsive (i.e., $S > 0$). To summarize, the moving or stationary bright (dark) solitary waves can be obtained by choosing different physical parameters. We next present various exact solitary wave solutions of Eq. (16). In the case of $PS > 0$, with $\omega_0 > 0$, we obtain the following dark solitary wave solution of Eq. (16):

$$\phi_d = \sqrt{\omega_0/|S|}(\cos\theta \tanh z_d + i \sin\theta), \quad (23)$$

where $z_d = \sqrt{\omega_0/|P|}[\cos\theta[X - X_0(T)]]$. Here θ is the solitary wave phase angle, $X_0(T)$ is the solitary wave center, and the solitary wave velocity is $dX_0/dT = \sqrt{\omega_0/|P|}\sin\theta$.

In the case of $PS < 0$, with $\omega_0 < 0$, the bright solitary wave solution of Eq. (16) is

$$\phi_b = \eta \operatorname{sech} z_b \exp(i\kappa X), \quad (24)$$

where $z_b = \eta \sqrt{-S/P}[X - X_0(T)]$. Here η is the solitary wave amplitude and satisfies the relation $\omega_0 = (\eta^2 S/P - \kappa^2)/2$, where $X_0(T)$ is the solitary wave center. The solitary wave velocity is connected to the wave number κ , i.e., $dX_0/dT = P\kappa$.

We next obtain the first-order approximate solitary wave solutions of the original Eqs. (2) and (3):

$$\begin{aligned} \begin{pmatrix} \psi_1 \\ \psi_2 \end{pmatrix} &\approx \begin{pmatrix} 1 \\ Q \end{pmatrix} \epsilon \sqrt{\omega_0/|S|} (\cos\theta \tanh z_d + i \sin\theta) \\ &\times \exp[i\kappa x - i(\omega + \epsilon^2 \omega_0)t], \end{aligned} \quad (25)$$

$$\begin{aligned} \begin{pmatrix} \psi_1 \\ \psi_2 \end{pmatrix} &\approx \begin{pmatrix} 1 \\ Q \end{pmatrix} \epsilon \eta \operatorname{sech} z_b \exp[i(k + \epsilon \kappa)x - i(\omega + \epsilon^2 \omega_0)t]. \end{aligned} \quad (26)$$

Here Eqs. (25) and (26) are the dark and bright solitary wave solutions, respectively.

IV. NUMERICAL RESULTS

A. Stability and dynamics of solitary waves

It is also important to research the stability of solitary waves. In the following, we will use two different approaches to examine the stabilities of the solitary waves. We first perform the linear stability analysis for the stationary solutions. Our analysis relies on the study of the Bogoliubov–de Gennes excitation spectrum around a stationary solitary wave solution $\varphi(x) = [\varphi_1(x), \varphi_2(x)]^T$ of Eqs. (2) and (3), with chemical potential μ . The spectrum is obtained as follows. We consider small perturbation to the solution $\psi(x, t)$, in the form

$$\psi_1(x, t) = \{\varphi_1(x) + \epsilon[e^{\lambda t} a_1(x) + e^{\lambda^* t} b_1^*(x)]\} e^{-i\mu t}, \quad (27)$$

$$\psi_2(x, t) = \{\varphi_2(x) + \epsilon[e^{\lambda t} a_2(x) + e^{\lambda^* t} b_2^*(x)]\} e^{-i\mu t}, \quad (28)$$

where $\epsilon \ll 1$, λ measures the growth rate of the perturbation instability, $a_{1,2}(x)$ and $b_{1,2}(x)$ are the perturbation eigenfunctions of the linearized eigenvalue problem, and “*” denotes complex conjugation. Substituting Eqs. (27) and (28) into Eqs. (2) and (3) and after a simplification, then we obtain that the linear stability of the solitary wave solutions obeys

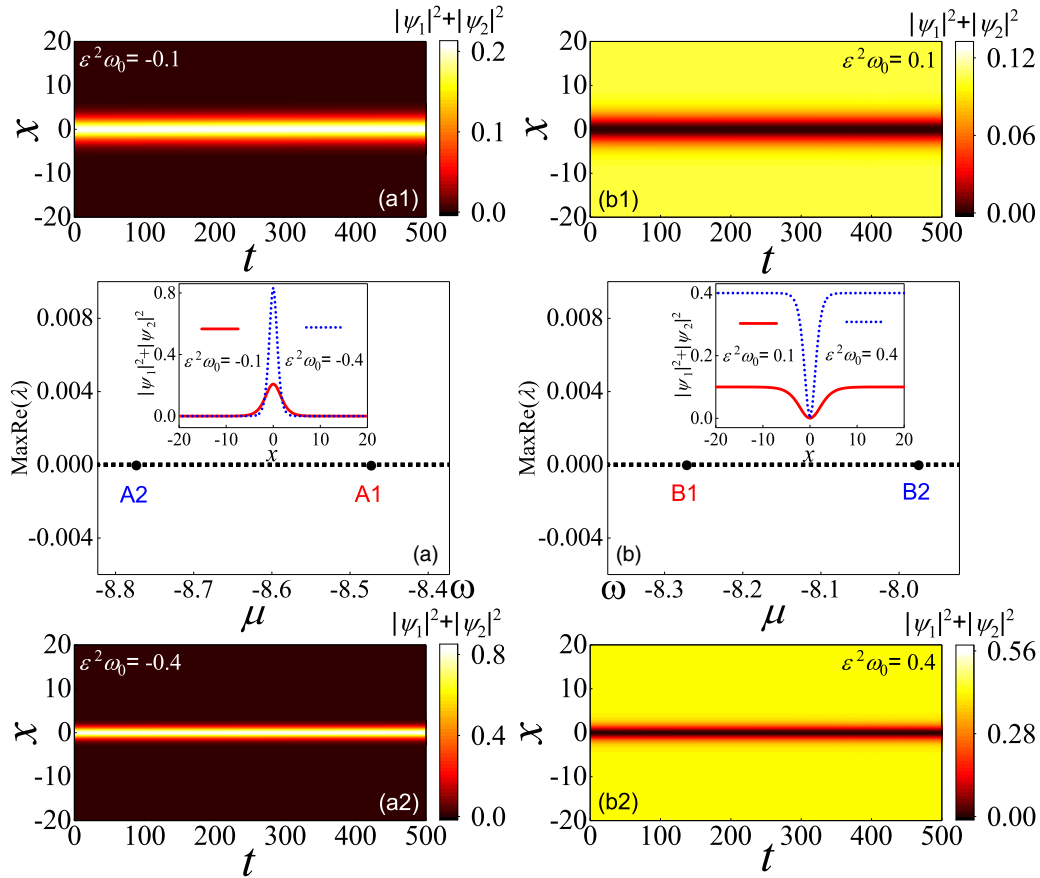


FIG. 5. The contour plots show the evolution of the total density for stationary solitary waves, bright solitary waves for $g_1 = g_2 = g_{12} = -1$, $\kappa = 0$ in (a1) and (a2) and dark solitary waves for $g_1 = g_2 = g_{12} = 1$, $\theta = 0$ in (b1) and (b2). The other parameters $\alpha = 1.5$, $\beta = 3$, $\Delta = 6$, and $k = -3.34$. [(a) and (b)] Maximum growth rates of perturbation as functions of the chemical potential for the stationary bright solitary wave and dark solitary wave, respectively. The insets in (a) and (b) are the density profiles of solitary waves at $t = 0$.

the following eigenvalue equations:

$$\begin{aligned}
 i\lambda a_1(x) &= \left[H_1 + i\beta \frac{\partial}{\partial x} \right] a_1(x) + g_1 \varphi_1^2(x) b_1(x) + \left[-i\alpha \frac{\partial}{\partial x} + g_{12} \varphi_1(x) \varphi_2^*(x) \right] a_2(x) + g_{12} \varphi_1(x) \varphi_2(x) b_2(x), \\
 i\lambda b_1(x) &= -g_1 \varphi_1^{*2}(x) a_1(x) + \left[-H_1 + i\beta \frac{\partial}{\partial x} \right] b_1(x) - g_{12} \varphi_1^*(x) \varphi_2^*(x) a_2(x) + \left[-i\alpha \frac{\partial}{\partial x} - g_{12} \varphi_1^*(x) \varphi_2(x) \right] b_2(x), \\
 i\lambda a_2(x) &= \left[-i\alpha \frac{\partial}{\partial x} + g_{12} \varphi_1^*(x) \varphi_2(x) \right] a_1(x) + g_{12} \varphi_1(x) \varphi_2(x) b_1(x) + \left[H_2 - i\beta \frac{\partial}{\partial x} \right] a_2(x) + g_2 \varphi_2^2(x) b_2(x), \\
 i\lambda b_2(x) &= -g_{12} \varphi_1^*(x) \varphi_2^*(x) a_1(x) + \left[-i\alpha \frac{\partial}{\partial x} - g_{12} \varphi_1(x) \varphi_2^*(x) \right] b_1(x) - g_2 \varphi_2^{*2}(x) a_2(x) + \left[-H_2 - i\beta \frac{\partial}{\partial x} \right] b_2(x), \quad (29)
 \end{aligned}$$

where $H_1 = -1/2\partial_{xx} + \Delta/2 + 2g_1|\varphi_1(x)|^2 + g_{12}|\varphi_2(x)|^2 - \mu$, $H_2 = -1/2\partial_{xx} - \Delta/2 + 2g_2|\varphi_2(x)|^2 + g_{12}|\varphi_1(x)|^2 - \mu$. The above linear eigenvalue problem (29) can be solved numerically by the help of Fourier collocation method [52]. If there exists eigenvalues λ (at least one) which satisfies $\text{Re}(\lambda) > 0$, then the solitary wave solutions are linearly unstable; otherwise, the solutions are stable. The stability of solitary waves is also confirmed numerically by the nonlinear dynamical evolution. The solitary wave solutions are added a perturbation with a noise of strength 5% of their initial amplitudes, which are used as the initial conditions for the

GP equations (2) and (3) and then numerically solved by the fourth-order Runge-Kutta method.

According to the above theoretical analysis, we not only obtain different types of the solitary waves but also study the stability of solitary waves. Figures 5 and 6 demonstrate the evolution of the total density $|\psi_1|^2 + |\psi_2|^2$ for the stationary and moving bright (dark) solitary waves and their linear stability analysis, respectively. In order to obtain the stationary solitary wave of the system, we select the appropriate parameters corresponding to bright or dark solitary waves with zero group velocity and zero solitary waves velocity. Here we use

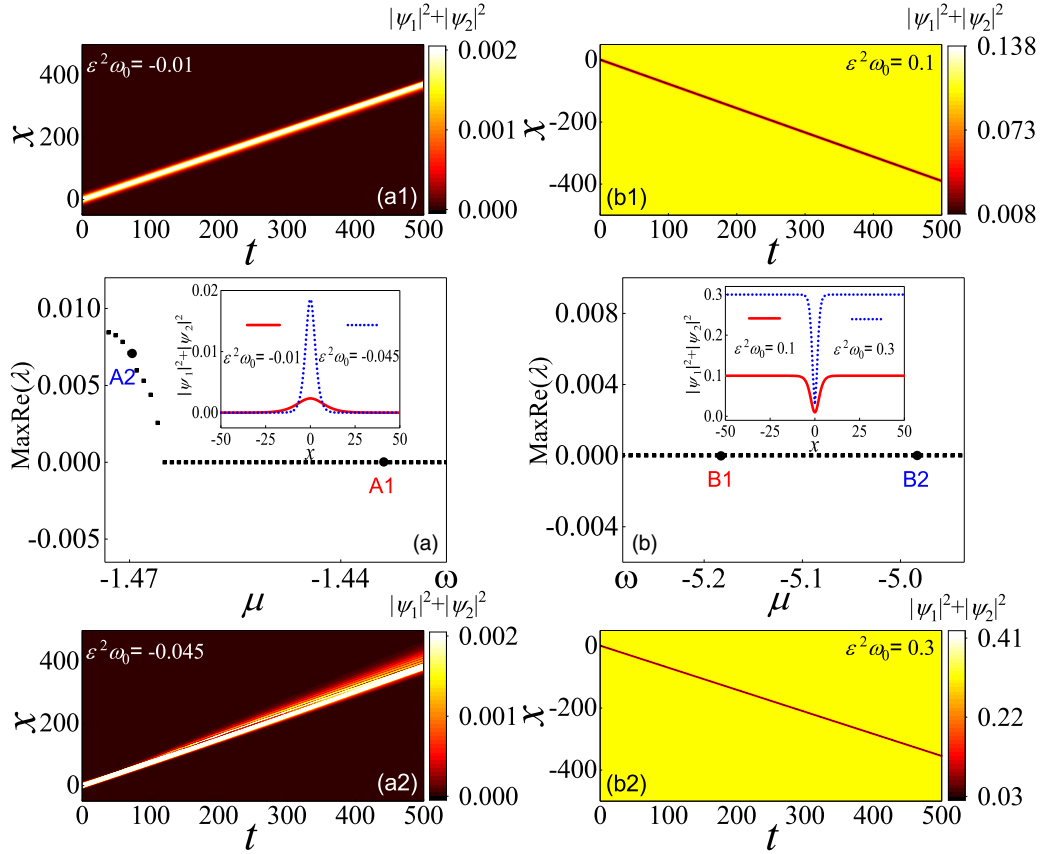


FIG. 6. The contour plots show the evolution of the total density for moving solitary waves, bright solitary waves for $\beta = 1.2$, $\kappa = 1$ in (a1) and (a2), dark solitary waves for $\beta = -2$, $\theta = \pi/10$ in (b1) and (b2). The other parameters $\alpha = 1.5$, $g_1 = g_2 = g_{12} = 1$, $\Delta = 6$ and $k = 1.5$. [(a) and (b)] Maximum growth rates of perturbation as functions of the chemical potential for the moving bright solitary wave and dark solitary wave respectively. The insets in (a) and (b) are the density profiles of solitary waves at $t = 0$.

the parameters $\alpha = 1.5$, $\beta = 3$, and $\Delta = 6$ in Fig. 5, and we can obtain that the solitary wave is stationary at $k = -3.34$ by solving Eq. (14) [see Fig. 2(a)]. Combining Fig. 4, when $g_1 = g_2 = g_{12} = -1$, there should be the stationary bright solitary waves in the system, as shown in Figs. 5(a1) and 5(a2); when $g_1 = g_2 = g_{12} = 1$, there should be the stationary dark solitary waves in the system, as shown in Figs. 5(b1) and 5(b2). Figures 5(a) and 5(b) illustrate the linear stability analysis of the stationary bright and dark solitary waves respectively by depicting the maximum value of $\text{Re}(\lambda)$ versus the chemical potential μ . It can be seen that $\text{MaxRe}(\lambda)$ of both stationary bright and dark solitary waves are zero in a reasonable range of chemical potential, i.e., these solitary waves are stable. And then we plot the corresponding solitary wave evolutions by selecting the points A1 ($\mu = -8.473$) and A2 ($\mu = -8.773$) in Fig. 5(a) and the points B1 ($\mu = -8.273$) and B2 ($\mu = -7.973$) in Fig. 5(b) [see Figs. 5(a1), 5(a2), 5(b1) and 5(b2)]. It is obviously that the shape, amplitude, and position of the stationary solitary waves do not change during the evolution process, indicating that these solitary waves are dynamically stable, which are in agreement with the results of linear stability analysis. Note that the insets in Figs. 5(a) and 5(b) are the total density profiles of solitary waves at $t = 0$. And it can be seen that with the increase of energy deviation $\epsilon^2\omega_0$, the amplitude of solitary wave increases and the wave width

decreases. In Fig. 6, we use parameters $\alpha = 1.5$, $k = 1.5$, $g_1 = g_2 = g_{12} = 1$, and $\Delta = 6$. From Fig. 3 and Fig. 4, when $\beta = 1.2$, it can be judged that there are moving bright solitary waves in the system and the group velocity $v > 0$, the solitary waves propagate in the positive direction. This is clearly shown in Figs. 6(a1) and 6(a2). Similarly, when $\beta = -2$, there are moving dark solitary waves in the system, and the solitary waves propagate in the negative direction ($v < 0$), which are shown in Figs. 6(b1) and 6(b2). Furthermore, the linear stability analyses of moving bright and dark solitary waves are shown in Figs. 6(a) and 6(b) by depicting $\text{MaxRe}(\lambda)$ versus μ . Here it can be observed from Fig. 6(a) that $\text{MaxRe}(\lambda) > 0$ occurs with certain μ , indicating that the bright solitary wave becomes unstable and is stable sufficiently close to the linear energy band ω . We also plot the bright solitary wave evolutions in Figs. 6(a1) and 6(a2) by selecting the points A1 ($\mu = -1.435$) and A2 ($\mu = -1.470$) in Fig. 6(a). It can be seen that the bright solitary wave evolution in Fig. 6(a1) is stable. However, it is apparent from Fig. 6(a2) that the bright solitary wave has a significant emission of radiation and distortion during the evolution process, which means that the bright solitary wave is unstable. These numerical results are consistent with the linear stability analysis. Similarly, from Fig. 6(b) and Figs. 6(b1) and 6(b2), the linear stability analysis and the dynamical evolution show that the moving dark solitary waves

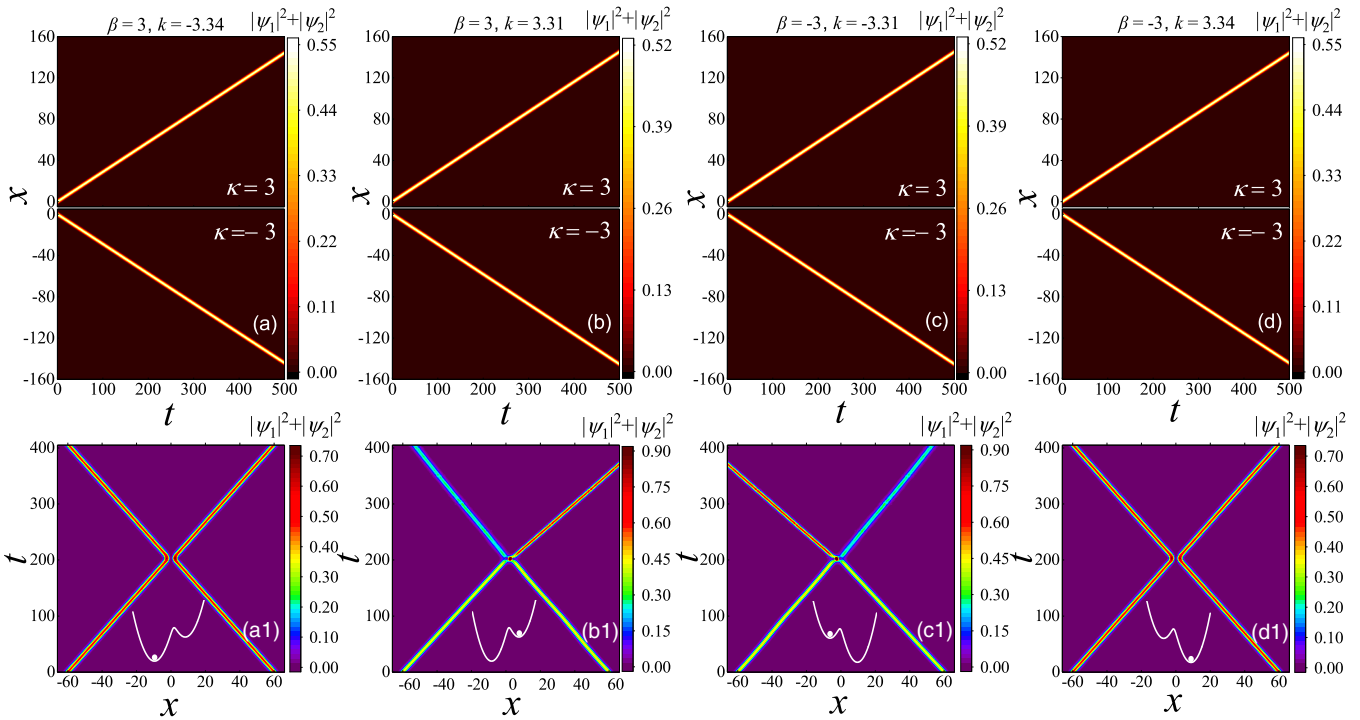


FIG. 7. The top row: The contour plots of the evolution of the total density for the moving solitary waves. The bottom row: Head-on collisions of the solitary waves which corresponds to the top row in the (x, t) plane, where $\kappa = 3$ ($\kappa = -3$) for all left-moving (right-moving) solitary waves. The insets in the bottom row are the schematic diagrams of the position of solitary wave states in the linear energy band. The other parameters $\alpha = 1.5$, $\Delta = 6$, $g_1 = g_2 = g_{12} = -1$, and $\epsilon^2 \omega_0 = -0.3$.

are stable within a reasonable chemical potential region. The insets in Figs. 6(a) and 6(b) are the total density profiles of solitary waves at $t = 0$. And the amplitude and wave width of the solitary waves with the increase of energy deviation $\epsilon^2 \omega_0$ also increase and decrease, respectively.

The above investigations indicate that our analytical results are in excellent agreement with the numerical results.

B. Collisions of solitary waves

Collisions are also one of the important dynamic properties of solitary waves, which have attracted extensive research interest [2,12,36]. In Fig. 7, we study the head-on collisions between two stable moving solitary waves in the system by taking the bright solitary waves as an example via the direct numerical simulation. We consider four pairs of solitary waves located at the four extremum points in the energy band structure of Fig. 1(b), which are $k = -3.34$ and $k = 3.31$ for $\beta = 3$ and $k = -3.31$ and $k = 3.34$ for $\beta = -3$, to study the head-on collisions between solitary waves. The top row of Fig. 7 demonstrates the dynamic evolution of each pair of bright solitary wave moving in opposite direction. It can be seen that all the solitary waves here are stable. Next, we place the each pair of solitary wave moving in opposite direction at the spatially symmetrical position at the initial time, so that they can have head-on collisions. The collision evolution results of the above four pairs of solitary waves are shown in bottom row of Fig. 7.

Figures 7(a1) and 7(d1) respectively show the collision scenarios when the solitary waves are at the minimum points $k =$

∓ 3.34 in the energy band of $\beta = \pm 3$ [see Fig. 1(b) and the insets in Figs. 7(a1) and 7(d1)]. It can be clearly observed that the velocity directions of the left-moving and right-moving solitary waves after collision are just opposite to the initial directions. Nevertheless, the parameters of the left-moving and right-moving solitary waves including the amplitude, width, and velocity magnitude do not change after collision, which remarkably indicate no energy exchange between them. That is the collisions of solitary waves in Figs. 7(a1) and 7(d1) are nearly elastic.

Figure 7(b1) shows the collision scenario when the solitary wave at another extremum point $k = 3.31$ in the energy band of $\beta = 3$ [see Fig. 1(b) and the inset in Fig. 7(b1)]. From Fig. 7(b1), it can be clearly seen that the left-moving and right-moving solitary waves pass through each other after collision, and the directions and the velocity magnitude of the two solitary waves both have obvious changes. Obviously, the velocity of the left-moving solitary wave becomes larger but the right-moving solitary wave becomes smaller. Moreover, the amplitude of the two solitary waves also have great changes after collisions. Concretely speaking, the amplitude of the left-moving solitary wave gets enhanced significantly, and at the same time the amplitude of the right-moving solitary wave diminishes significantly, which means that there is an energy exchange between the two solitary waves. These indicate that the collision in Fig. 7(b1) is inelastic. Interestingly, the evolution of solitary waves after collision is also related to the right-handed and left-handed helicoidal gauge potential. Figure 7(c1) shows the collision scenario when the solitary wave at the extremum point $k = -3.31$ in the energy band of

$\beta = -3$ [see Fig. 1(b) and the inset in Fig. 7(c1)]. We can observe that the solitary wave collision here is also inelastic and the change of motion trajectory and the amplitude for the left-moving and right-moving solitary waves are just opposite to those in Fig. 7(b1).

The above numerical results show that in this system, the interactions between solitary waves have both elastic and inelastic collisions, which are closely related to the position of solitary wave states in the linear energy band. It is easy to excite elastic collision when solitary waves are at the minimum point in the energy band, while the inelastic collision can be excited when solitary waves are at another asymmetric extremum point.

V. CONCLUSIONS

In summary, we investigated the different types of the solitary wave in the two-component helicoidal spin-orbit coupled BECs by using the multiscale perturbation method. A single NLS equation was derived and the solitary wave solutions of the system were obtained. Our analysis indicates that the helicoidal gauge potential breaks the symmetry of the energy band and adjusts the energy band structure, thus further affecting solitary wave excitation in the system. Furthermore, the analytical prediction of different solitary waves (i.e., stationary or moving or bright or dark solitary waves) of the system in parameter space was also given. In particular, the helicoidal gauge potential changes the solitary wave types drastically for the weak spin-orbit coupling, i.e., when in the absence of the helicoidal gauge potential, only dark (bright) solitary wave solutions exist in the system with repulsive (attractive) atomic interaction; however, when in the presence of the helicoidal gauge potential, both dark and bright solitary

wave solutions can exist in the system regardless of whether the atomic interaction is repulsive or attractive. In addition, we investigated the stability of solitary wave and obtained the stability regions of different types of solitary waves by applying the linear stability analysis. It is found that in such a nonlinear system, the stationary solitary waves are stable, and there are both stable and unstable moving solitary waves. Among them, the moving bright solitary waves is stable when the chemical potential is sufficiently close to the linear energy band. The dynamic evolution results of the solitary waves by the direct numerical simulation not only validate the linear stability analysis, but also confirm the analytical prediction for the solitary wave types. Finally, the collision effects between solitary waves were also displayed by the numerical simulation. It is shown that the interactions between solitary waves in the system have both elastic and inelastic collisions, which are closely related to the position of solitary wave states in the linear energy band. It is easy to excite elastic collision when solitary waves are at the minimum point in the energy band, while the inelastic collision can be excited when solitary waves are at another asymmetric extremum point. Our results provide a potential way to adjust the types of solitary waves in BECs with helicoidal gauge potential.

ACKNOWLEDGMENTS

This work is supported by the National Natural Science Foundation of China under Grants No. 11764039, No. 11847304, No. 11865014, No. 11475027, No. 11305132, and No. 11274255; by Natural Science Foundation of Gansu province under Grant No. 17JR5RA076; and by Scientific research project of Gansu higher education under Grant No. 2016A-005.

-
- [1] Y. V. Kartashov, B. A. Malomed, and L. Torner, *Rev. Mod. Phys.* **83**, 247 (2011).
 - [2] A. D. Martin, C. S. Adams, and S. A. Gardiner, *Phys. Rev. Lett.* **98**, 020402 (2007).
 - [3] A. Chabchoub, O. Kimmoun, H. Branger, N. Hoffmann, D. Proment, M. Onorato, and N. Akhmediev, *Phys. Rev. Lett.* **110**, 124101 (2013).
 - [4] P. K. Shukla and B. Eliasson, *Phys. Rev. Lett.* **96**, 245001 (2006).
 - [5] B. Wetzell, D. Bongiovanni, M. Kues, Y. Hu, Z. G. Chen, S. Trillo, J. M. Dudley, S. Wabnitz, and R. Morandotti, *Phys. Rev. Lett.* **117**, 073902 (2016).
 - [6] J. Li, D. S. Wang, Z. Y. Wu, Y. M. Yu, and W. M. Liu, *Phys. Rev. A* **86**, 023628 (2012).
 - [7] Y. S. Kivshar and B. A. Malomed, *Rev. Mod. Phys.* **61**, 763 (1989).
 - [8] T. M. Bersano, V. Gokhroo, M. A. Khamehchi, J. D'Ambrose, D. J. Frantzeskakis, P. Engels, and P. G. Kevrekidis, *Phys. Rev. Lett.* **120**, 063202 (2018).
 - [9] J. H. V. Nguyen, D. Luo, and R. G. Hulet, *Science* **356**, 422 (2017).
 - [10] K. E. Strecker, G. B. Partridge, A. G. Truscott, and R. G. Hulet, *Nature (Lond.)* **417**, 150 (2002).
 - [11] P. Öhberg and L. Santos, *Phys. Rev. Lett.* **86**, 2918 (2001).
 - [12] X. F. Zhang, X. H. Hu, X. X. Liu, and W. M. Liu, *Phys. Rev. A* **79**, 033630 (2009).
 - [13] T. Busch and J. R. Anglin, *Phys. Rev. Lett.* **87**, 010401 (2001).
 - [14] I. Danaila, M. A. Khamehchi, V. Gokhroo, P. Engels, and P. G. Kevrekidis, *Phys. Rev. A* **94**, 053617 (2016).
 - [15] V. Achilleos, D. J. Frantzeskakis, P. G. Kevrekidis, and D. E. Pelinovsky, *Phys. Rev. Lett.* **110**, 264101 (2013).
 - [16] Y. Xu, Y. P. Zhang, and B. Wu, *Phys. Rev. A* **87**, 013614 (2013).
 - [17] V. Achilleos, J. Stockhofe, P. G. Kevrekidis, D. J. Frantzeskakis, and P. Schmelcher, *Europhys. Lett.* **103**, 20002 (2013).
 - [18] Y. V. Kartashov, V. V. Konotop and F. Kh. Abdullaev, *Phys. Rev. Lett.* **111**, 060402 (2013).
 - [19] V. E. Lobanov, Y. V. Kartashov, and V. V. Konotop, *Phys. Rev. Lett.* **112**, 180403 (2014).
 - [20] Y. Y. Li, Y. Liu, Zh. W. Fan, W. Pang, Sh. H. Fu, and B. A. Malomed, *Phys. Rev. A* **95**, 063613 (2017).
 - [21] H. Takeuchi, *Phys. Rev. A* **97**, 013617 (2018).
 - [22] O. Fialko, J. Brand, and U. Zülicke, *Phys. Rev. A* **85**, 051605(R) (2012).
 - [23] H. Sakaguchi, E. Ya. Sherman, and B. A. Malomed, *Phys. Rev. E* **94**, 032202 (2016).

- [24] B. A. Malomed, *Europhys. Lett.* **122**, 36001 (2018).
- [25] B. A. Malomed, *Physica D* **399**, 108 (2019).
- [26] V. Achilleos, D. J. Frantzeskakis, P. G. Kevrekidis, P. Schmelcher, and J. Stockhofe, *Rom. Rep. Phys.* **67**, 235 (2015).
- [27] Y. E. Li and J. K. Xue, *Front. Phys.* **13**, 130307 (2018).
- [28] N. S. Wan, Yu.-E. Li, and J. K. Xue, *Phys. Rev. E* **99**, 062220 (2019).
- [29] J. Ruseckas, G. Juzeliūnas, P. Öhberg, and M. Fleischhauer, *Phys. Rev. Lett.* **95**, 010404 (2005).
- [30] Y. J. Lin, K. Jiménez-García, and I. B. Spielman, *Nature (Lond.)* **471**, 83 (2011).
- [31] V. Galitski and I. B. Spielman, *Nature (Lond.)* **494**, 49 (2013).
- [32] D. R. Murray, P. Öhberg, D. Gomila, and S. M. Barnett, *Phys. Rev. A* **79**, 063618 (2009).
- [33] S. S. S. Hejazi, J. Polo, R. Sachdeva, and T. Busch, *Phys. Rev. A* **102**, 053309 (2020).
- [34] Y. V. Kartashov, V. V. Konotop, and D. A. Zezyulin, *Phys. Rev. A* **90**, 063621 (2014).
- [35] Y. V. Kartashov, V. V. Konotop, M. Modugno, and E. Ya. Sherman, *Phys. Rev. Lett.* **122**, 064101 (2019).
- [36] Y. V. Kartashov and V. V. Konotop, *Phys. Rev. Lett.* **118**, 190401 (2017).
- [37] Y. V. Kartashov, E. Ya. Sherman, B. A. Malomed, and V. V. Konotop, *New J. Phys.* **22**, 103014 (2020).
- [38] J. Struck, C. Ölschläger, M. Weinberg, P. Hauke, J. Simonet, A. Eckardt, M. Lewenstein, K. Sengstock, and P. Windpassinger, *Phys. Rev. Lett.* **108**, 225304 (2012).
- [39] Y. Zhang, G. Chen, and C. Zhang, *Sci. Rep.* **3**, 1937 (2013).
- [40] K. Jiménez-García, L. J. LeBlanc, R. A. Williams, M. C. Beeler, C. Qu, M. Gong, C. Zhang, and I. B. Spielman, *Phys. Rev. Lett.* **114**, 125301 (2015).
- [41] X. Luo, L. Wu, J. Chen, Q. Guan, K. Gao, Z. F. Xu, L. You, and R. Wang, *Sci. Rep.* **6**, 18983 (2016).
- [42] S.-W. Su, S.-C. Gou, I.-K. Liu, I. B. Spielman, L. Santos, A. Acus, A. Mekys, J. Ruseckas, and G. Juzeliunas, *New J. Phys.* **17**, 033045 (2015).
- [43] M. C. Rechtsman, J. M. Zeuner, Y. Plotnik, Y. Lumer, D. Podolsky, F. Dreisow, S. Nolte, M. Segev, and A. Szameit, *Nature (Lond.)* **496**, 196 (2013).
- [44] X. X. Li, R. J. Cheng, A. X. Zhang, and J. K. Xue, *Phys. Rev. E* **100**, 032220 (2019).
- [45] S. Blatt, T. L. Nicholson, B. J. Bloom, J. R. Williams, J. W. Thomsen, P. S. Julienne, and J. Ye, *Phys. Rev. Lett.* **107**, 073202 (2011).
- [46] S. Inouye, M. R. Andrews, J. Stenger, H.-J. Miesner, D. M. Stamper-Kurn, and W. Ketterle, *Nature (Lond.)* **392**, 151 (1998).
- [47] S. V. Samsonov, A. D. R. Phelps, V. L. Bratman, G. Burt, G. G. Denisov, A. W. Cross, K. Ronald, W. He, and H. Yin, *Phys. Rev. Lett.* **92**, 118301 (2004).
- [48] G. Burt, S. V. Samsonov, K. Ronald, G. G. Denisov, A. R. Young, V. L. Bratman, A. D. R. Phelps, A. W. Cross, I. V. Konoplev, W. He, J. Thomson, and C. G. Whyte, *Phys. Rev. E* **70**, 046402 (2004).
- [49] J. Denschlag, J. E. Simsarian, and D. L. Feder, *Science* **287**, 97 (2000).
- [50] S. Burger, K. Bongs, S. Dettmer, W. Ertmer, K. Sengstock, A. Sanpera, G. V. Shlyapnikov, and M. Lewenstein, *Phys. Rev. Lett.* **83**, 5198 (1999).
- [51] A. Jeffrey and T. Kawahara, *Asymptotic Methods in Nonlinear Wave Theory* (Pitman, Boston, 1982).
- [52] J. K. Yang, *Nonlinear Waves in Integrable and Nonintegrable Systems* (SIAM, Philadelphia, PA, 2010).